Environmental Science and Pollution Research (2019) 26:36096–36106
https://doi.org/10.1007/s11356-019-04474-x

SOLAR CHEMISTRY AND PHOTOCATALYSIS: ENVIRONMENTAL APPLICATIONS

Copper-doped TiO_2 photocatalysts: application to drinking water by humic matter degradation

Nazli Turkten[1,2] · Zekiye Cinar[3] · Ayse Tomruk[1] · Miray Bekbolet[1]

Received: 28 July 2018 / Accepted: 4 February 2019 / Published online: 27 February 2019

Abstract

The aim of this study was to determine the photocatalytic performance of copper-doped TiO_2 (Cu-TiO_2) specimens on the degradation of dissolved organic matter (DOM) represented by a model humic acid (HA). TiO_2 was synthesized by sol-gel method from an alkoxide precursor. Cu-doped TiO_2 specimens containing 0.25 wt% and 0.50 wt% Cu were prepared by wet impregnation method using sol-gel synthesized as well as bare TiO_2 P-25 and characterized by XRD, SEM, XPS, Raman spectroscopy, UV-DRS, and BET measurements. Their photocatalytic activities were evaluated with regard to degradation kinetics of HA in terms of UV-vis and fluorescence spectroscopic parameters and organic contents. HA fluorescence excitation emission matrix (EEM) contour plots indicated that the solar photocatalytic degradation pathway was TiO_2-type specific and Cu dopant content.

Keywords Cu-doped TiO_2 · EEM · Humic acid · Photocatalysis · Sol-gel · TiO_2

Introduction

It is widely known that the presence of DOM in natural water poses severe problems even after the application of appropriate treatment options, i.e. conventional treatment followed by specific processes for disinfection of microorganisms. Due to widely applied chlorine-based chemical oxidation, or ozonation and even by UV-irradiation, formation of undesirable disinfection by-products expresses significant public health concerns. Therefore, successful removal of allochthonous (watershed or terrestrial origin) and/or autochthonous (algal or in situ-formed) organic matter in water should be achieved to fulfill the requirements of safe drinking water to consumers. Organic content of DOM is defined as 0.45 μm filtered fraction (DOC) that is comprised of diverse molecular size fractions (< 0.45 μm filtered fraction to < 500 Da) each composed of different sub-components. Major fraction of DOM is defined as HA expressing more dense aromatic content and lower molecular size fractions are mostly fulvic like organics (FA) displaying more aliphatic character and rich in functional groups.

Titanium dioxide (TiO_2) photocatalysis has gained great attention in past several decades as a promising advanced oxidation process. Photocatalytic degradation of DOM and model compounds such as HAs and FAs has been studied extensively by Bekbolet and colleagues using black light fluorescent lamps ($\lambda_{max} = 365$ nm) as the light source (Tercero Espinoza et al. 2011; Uyguner-Demirel and Bekbolet 2011; Uyguner and Bekbolet 2004; Uyguner and Bekbolet 2007). The wide band-gap of TiO_2 ($E_{bg} = 3.2$ eV for anatase and brookite and $E_{bg} = 3.0$ eV for rutile) indicates an excitation wavelength in the UV region that also coincides with ~ 5% of the solar spectrum (Kumar and Devi 2011). To improve the utilization of TiO_2 photocatalyts, efficiently under visible light irradiation, various strategies such as metal ion doping, anion doping, co-doping, and surface sensitization by organic dyes have been developed (Banerjee et al. 2014; Chelli and Golder 2017; Etacheri et al. 2015; Fagan et al. 2016; Fisher et al.

Responsible editor: Suresh Pillai

Electronic supplementary material The online version of this article (https://doi.org/10.1007/s11356-019-04474-x) contains supplementary material, which is available to authorized users.

✉ Miray Bekbolet
bekbolet@boun.edu.tr

[1] Institute of Environmental Sciences, Bogazici University, Bebek, 34342 Istanbul, Turkey

[2] Present address: Department of Chemistry, Faculty of Science and Arts, Kirsehir Ahi Evran University, 40100 Kirsehir, Turkey

[3] Department of Chemistry, Yildiz Technical University, 34220 Istanbul, Turkey

2013; Pelaez et al. 2012). Selective doping of metal ions (Mn^{2+}, Fe^{3+}, Cr^{3+}, Cu^{2+}) has been shown to be effective in improving visible light activity (Kumar and Devi 2011). For this reason, copper has been extensively used as a dopant in the synthesis of metal-doped TiO_2 with reduced band gap and enhanced photocatalytic activity. Pioneering works on Cu doping reported the use of Degussa P-25 or sol-gel prepared catalysts with copper loadings by wet impregnation, chemisorption-hydrolysis and by in situ methods (Boccuzzi et al. 1997; Bokhimi et al. 1997; Coloma et al. 2000; Colón et al. 2006). Since then, most of the interest was directed to "material preparation and activity testing type" studies (Aguilar et al. 2013; López et al. 2009; Pongwan et al. 2016; Tseng et al. 2002). A brief literature survey (2013–2018) on this topic revealed numerous publications from which selected samples were compiled and evaluated in Table 1 in Supplementary Information (SI) part 1. Cu-doped TiO_2 has been prepared and applied specifically for H_2 production (Bashiri et al. 2015; Hu et al. 2016; Jo and Jin 2018; Mahmoud et al. 2018; Polliotto et al. 2018; Praveen Kumar et al. 2016; Zhang et al. 2016). Activity testing studies were mainly performed using various dyes as methylene blue (Aguilar et al. 2013; Bensouici et al. 2017; Dong et al. 2018; Hirota and Maeda 2017; Jaiswal et al. 2015; Moongraksathum et al. 2018; Pava-Gómez et al. 2018; Reda et al. 2017; Wang et al. 2018), Congo red (Golder 2017; Unwiset et al. 2018), and methyl orange (Dorraj et al. 2017; Reda et al. 2017; Yang et al. 2015). Several specific chemical compounds as an example of antibiotics (tetracycline hydrochloride, (Cao et al. 2018)), pesticides (Ci et al. 2018), p-nitrophenol (Yang et al. 2015), 2-chloropenol (Lin et al. 2018), and chlorinated solvents (Biyoghe Bi Ndong et al. 2014) were also considered. Applications to real wastewaters or drinking waters as well as photocatalytic disinfection of microorganisms, i.e., *Escherichia coli*, bacteriophage f2, and *Staphylococcus aureus* (Guo et al. 2017; Karunakaran et al. 2010; Khraisheh et al. 2015; Leyland et al. 2016; Mathew et al. 2018; Moongraksathum et al. 2018; Zheng et al. 2018), have also been reported. Recent interest is extended to the use of Cu-doped TiO_2 prepared by sol-gel method for elucidation of oxidative stress–mediated cytotoxicity in human lung epithelial A549 cells (Ahmad et al. 2018).

Aqueous Cu species expressed a retardation effect on the photocatalytic treatment of humic acids and molecular size fractions (0.45 μm filtered fraction, and 100 kDa fraction). An enhancement was recorded for fraction comprised of molecular size < 30 kDa compounds (Uyguner and Bekbolet 2010). The retardation effect of copper ions was related to the molecular size changes in NOM due to the selective degradation mechanism (Tercero Espinoza et al. 2011). Cu ions in aqueous solution could bind to both humic molecular size fractions and photocatalyst particles via binary and ternary adsorptive interactions leading to various different mechanisms of degradation (Uyguner and Bekbolet 2010). Cu-doped TiO_2 surface could express different sites for adsorptive interactions with humic molecular size fractions (Araña et al. 2005; Yang et al. 2015).

This study was performed aiming to elucidate the performance of sol-gel synthesized Cu-doped TiO_2 for photocatalytic treatment of humic acid comprised of fractions expressing < 30 kDa molecular size. TiO_2 P-25, TiO_2 prepared by sol-gel method, and respective Cu-doped specimens were investigated under identical experimental conditions.

Methodology

Photocatalyst specimens

TiO_2 P-25 powder (Evonik) was used (referred to as TiO_2). Sol-gel TiO_2 (synTiO_2) was synthesized using a sol-gel method previously developed and described (Turkten and Cinar 2017). Doping was performed by an incipient wet impregnation method using $Cu(NO_3)_2{\cdot}3H_2O$ as Cu source. Two different Cu-doped photocatalysts containing 0.25 wt% Cu (0.25% Cu-TiO_2) and 0.50 wt% Cu (0.50% Cu-TiO_2) were prepared by using TiO_2 as well as synTiO_2 (0.25% Cu-synTiO_2 and 0.50% Cu-synTiO_2). All Cu-doped TiO_2 samples were calcined at 773 K for 5 h and grinded.

Table 1 Properties of photocatalyst specimens

Photocatalyst specimen	Crystallite size, nm	Band gap energy/ wavelength eV/nm	BET surface area, m^2/g	Pore volume, cm^3/g	Pore size, nm	Anatase/rutile, %
TiO_2	42.44	3.18/390	57.56	0.150	16.75	79/21
SynTiO_2	33.14	2.91/426	50.25	0.169	4.442	87/13
0.25% Cu-TiO_2	20.32	2.98/416	46.69	0.0510	1.645	86/14
0.50% Cu-TiO_2	20.12	2.90/428	46.50	0.0512	1.492	84/16
0.25% Cu-synTiO_2	16.23	2.86/434	55.29	0.110	5.120	98/2
0.50% Cu-synTiO_2	17.01	2.82/440	44.22	0.0938	3.336	97/3

Characterization techniques

X-ray diffraction (XRD) patterns were recorded on a Rigaku-D/MAX-Ultima diffractometer. Crystallite size (*d*) was determined using the Scherrer equation. Scanning electron microscopy (SEM) was employed on an ESEM-FEG/EDAX Philips XL-30 instrument operating at 20 kV using catalyst powders supported on carbon tape. X-ray photoelectron spectroscopy (XPS) were performed on a Thermo Scientific K-Alpha x-ray photoelectron spectrometer. Raman spectra were acquired by a Renishaw inVia Microscope Raman spectrometer. UV-vis diffuse reflectance spectra (UV-vis DRS) were obtained using a UV-vis spectrophotometer (UV-2450, Shimadzu). Band gap energies of the photocatalyst specimens were calculated through the use of the Kubelka-Munk formula and Tauc equation. Detailed information on the applied methods were presented in SI Part 2. BET analysis and pore size was measured by BJH method of adsorption. Point of zero charge condition of the specimens were determined by pH dependent zeta potential measurements (Nanosizer Nano ZS (Malvern).

Humic acid

Thirty kilodalton molecular size fraction of HA was prepared using 50 mg/L HA that was filtered through 0.45 μm membrane filter (Millipore) followed by ultrafiltration using (Amicon 8050) ultrafiltration stirred cell unit (Kerc et al. 2004). Spectroscopic measurements were performed by using Perkin Elmer Lambda 35 UV-vis double beam spectrophotometer and Perkin Elmer LS 55 luminescence spectrometer (Uyguner-Demirel and Bekbolet 2011). UV-vis spectroscopic parameters were $Color_{436}$, UV_{365}, UV_{280}, and UV_{254}. Fluorescence spectroscopic parameters were fluorescence index (FI) and excitation emission matrix (EEM) fluorescence contour plots. Carbon-based UV-vis parameters as $CbColor_{436}$, $CbUV_{365}$, $CbUV_{280}$, and $CbUV_{254}$ as well as specific fluorescence index (SFI) were expressed by normalizing the respective spectroscopic parameters to DOC contents. Detailed information regarding spectroscopic analysis were presented in SI Part 3.4. DOC (mg/L) was determined as non-purgeable organic carbon by using total organic carbon analyzer Shimadzu TOC VWP.

Solar photocatalytic treatment

Solar photocatalysis were achieved by ATLAS Suntest CPS+ simulator equipped with an air cooled Xenon lamp (250 W/m^2 and wavelength range of 300–800 nm) as the light source (Ref. 56052371, Atlas CPS+ solar simulator). Photocatalyst specimens were removed from the reaction medium by immediate filtration through a 0.45-μm membrane filter. Clear samples were subjected to UV-vis and fluorescence spectroscopic analysis as well as DOC.

Results and discussion

Characterization of photocatalyst specimens

XRD patterns of TiO_2 specimens showed the presence of both anatase and rutile phases (Fig. 1 A–B). Six distinctive peaks corresponding to (1 0 1), (0 0 4), (2 0 0), (2 1 1), (1 1 8), and (1 1 6) planes of anatase were found. Peak at 25.5° (2θ) corresponded to the characteristic peak of (1 0 1) plane in anatase and at 27.7° (2θ) corresponded to the characteristic peak of (1 1 0) of rutile. XRD diffractograms of Cu-TiO_2 were identical to that of TiO_2. Cu-synTiO_2 diffractograms indicated predominantly anatase phase with a trace portion of rutile. The reason could be explained that Cu has a promoting effect on the transformation of anatase to rutile crystalline phase (Ilkhechi et al. 2015). All XRD diffractograms displayed typical peaks of anatase and rutile without any detectable Cu-related peaks revealing that Cu (II) ions did not react with TiO_2 to form new crystalline phases. Cu might have moved into the substitutional sites of the TiO_2 crystal structure. Cu-doped TiO_2 peaks slightly broadened indicating a reduction in the crystallite size thus average crystallite sizes were smaller than that of the undoped TiO_2 samples signifying a slight distortion in the crystal structure (Table 1). Substitution of Ti^{4+} cations by Cu^{2+} ions caused slight distortions via formation of crystallographic point defects. Formation of Cu–O–Ti could possibly inhibit the growth of crystal grains (Ilkhechi and Kaleji 2014). A slight shift in the peak position corresponding to (1 0 1) plane of anatase to a lower angle was observed indicating that the crystal was distorted by the incorporation of the dopants. Due to a smaller ionic radius (0.58 Å) of Cu^{2+} ion than Ti^{4+} ion (0.66 Å), substitution of Cu for Ti in TiO_2 crystal lattice resulted in a decrease in the interplanar distance. The conclusion was that substitutional doping of Cu^{2+} occurred instead of interstitial doping.

SEM micrographs indicated that all samples were consisted of small, nearly spherical, and some larger elongated particles (SI, Part 2, Fig. 1 A–F). A more rugged surface and smaller particles were observed in 0.50% Cu-synTiO_2 than 0.25% Cu-synTiO_2 sample. Thus, more active sites were thought to have been formed for the smaller particles on the synthesized TiO_2 when large amounts of dopant were used (Lin et al. 2018). Aggregation of particles could be visualized due to impurity doping leading to the formation of new defects and dislocations in the crystal lattice. Size of Cu-synTiO_2 particles were smaller than that of the undoped TiO_2 particles as compatible with the average crystallite particle sizes obtained from the Scherrer equation (Table 1).

Raman spectra of the samples and respective information were presented in SI, Part 2, Fig. 2. Raman peaks were observed at 142 (E_g), 394 (B_{1g}), 514 (E_g), and 637 (E_g) cm^{-1} in the spectra of all the samples, indicating that anatase nanoparticles are the predominant species (Li Bassi et al. 2005; Byrne

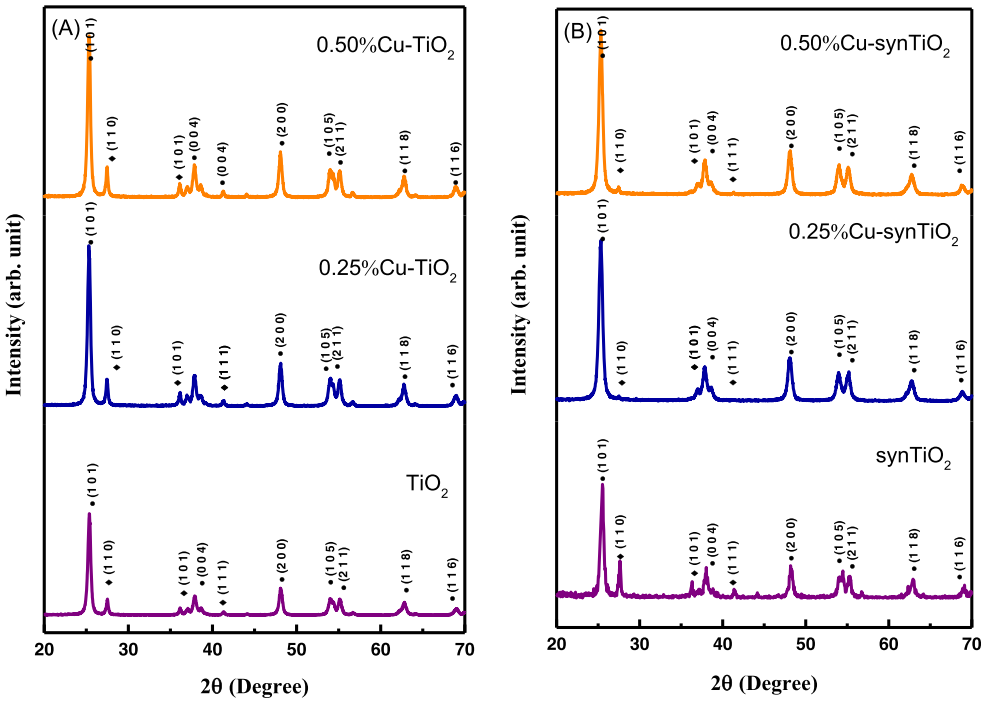

Fig. 1 XRD diffractograms (**a**) TiO_2 and Cu-TiO_2, (**b**) synTiO_2 and Cu-synTiO_2 (• anatase, ♦ rutile)

et al. 2016). On the other hand, E_g mode of rutile phase at 442 cm^{-1} was only observed in undoped TiO_2 samples and could not be detected in copper-doped samples. The presence of copper/copper oxides or other impurities were not noticed in Raman spectra. Thus confirms the presence of the dopant cation in the substitutional positions of the crystal lattice. Raman results could be assessed as consistent with the XRD measurements.

Characteristic peaks of Ti 2p, O 1s, and Cu 2p were evident in all samples as displayed by XPS diffractograms (Figure 2). Two peaks at ca. 458 eV and 463 eV corresponded to the photo-splitting electrons Ti $2p_{3/2}$ and Ti $2p_{1/2}$ indicating the presence of Ti^4. O 1s binding energies of Cu-synTiO_2 were located at a higher energy than 529.3 eV of synTiO_2 which was assigned to the metallic oxide (O_2^-) in the TiO_2 lattice. Peaks of Cu $2p_{3/2}$ and Cu $2p_{1/2}$ appeared at around 933 and 953 eV respectively confirming the presence of Cu^{2+} (Dorraj et al. 2018; Moongraksathum et al. 2018) No evidence of the presence of Cu^+ and Cu^0 were detected. The small change in the binding energy of Ti atom clearly showed the substitutions of few sites of Ti^{4+} ion by Cu^{2+} ions (Yadav et al. 2014). In the XPS spectrum of Cu-doped samples, Ti $2p_{3/2}$ peak displays higher binding energy than undoped TiO_2 samples. This small shift to higher binding energy indicates that the electronic interaction of Ti with Cu^{2+} ions is different in Cu-doped TiO_2 samples from that of the undoped TiO_2 samples. The reason of this slight shift is the presence of copper in lattice and this may be attributed to the formation of the Ti–O–Cu bonds in the crystal lattice (Carvalho et al. 2013; Jung et al. 2016; Mathew et al. 2018; Xu et al. 2008). C 1s spectra, N 1s spectra and survey spectra of TiO_2 samples were presented in SI, Part 2, Fig. 3. The deconvoluted Cu 2p and O 1s spectra of Cu-doped TiO_2 samples were also displayed in SI, Part 2, Fig. 4 and Fig. 5, respectively.

UV-DRS spectra of the undoped specimens had an absorption edge at around 410 nm; however, the absorption threshold of Cu-doped specimens shifted towards the visible region as 420 nm–600 nm (Fig. 3). This absorption edge indicated that Cu^{2+} ions were localized in the TiO_2 lattice occupying Ti^{4+} positions. Band gap energies and respective effective wavelengths indicated a red shift to possible use of solar irradiation. E_{bg}'s were $TiO_2 = 3.18$ eV ($\lambda = 390$ nm); syn$TiO_2 = 2.91$ eV ($\lambda = 426$ nm); 0.25% Cu-$TiO_2 = 2.98$ eV ($\lambda = 416$ nm); 0.50% Cu-$TiO_2 = 2.90$ eV ($\lambda = 428$ nm); 0.25% Cu-syn$TiO_2 = 2.86$ eV ($\lambda = 434$ nm); 0.50% Cu-syn$TiO_2 = 2.82$ eV ($\lambda = 440$ nm).

BET surface areas and pore volumes of Cu-TiO_2 samples were lower than TiO_2 (Table 1). On the other hand, a non-consistent trend was observed for synTiO_2. An increase in Cu-doping concentration, decreased surface area of 0.5% Cu-synTiO_2 to 44 m^2/g, the reason could be explained by the aggregation of smaller crystallites forming smaller pores or insertion Cu^{2+} ions into the pore of pure TiO_2 (López et al. 2009; Zhou et al. 2006). This is consistent with the SEM micrographs of 0.50% Cu-synTiO_2 which also showed tendency of aggregation. Through TEM measurements, separate existence of agglomerates of anatase and rutile particles in TiO_2 P-25 (Degussa) powder was reported (Ohno et al. 2001). Under operational conditions of photocatalysis, the agglomerates were expected to be dispersed keeping the anatase particles and rutile particles in contact. This mixed structure

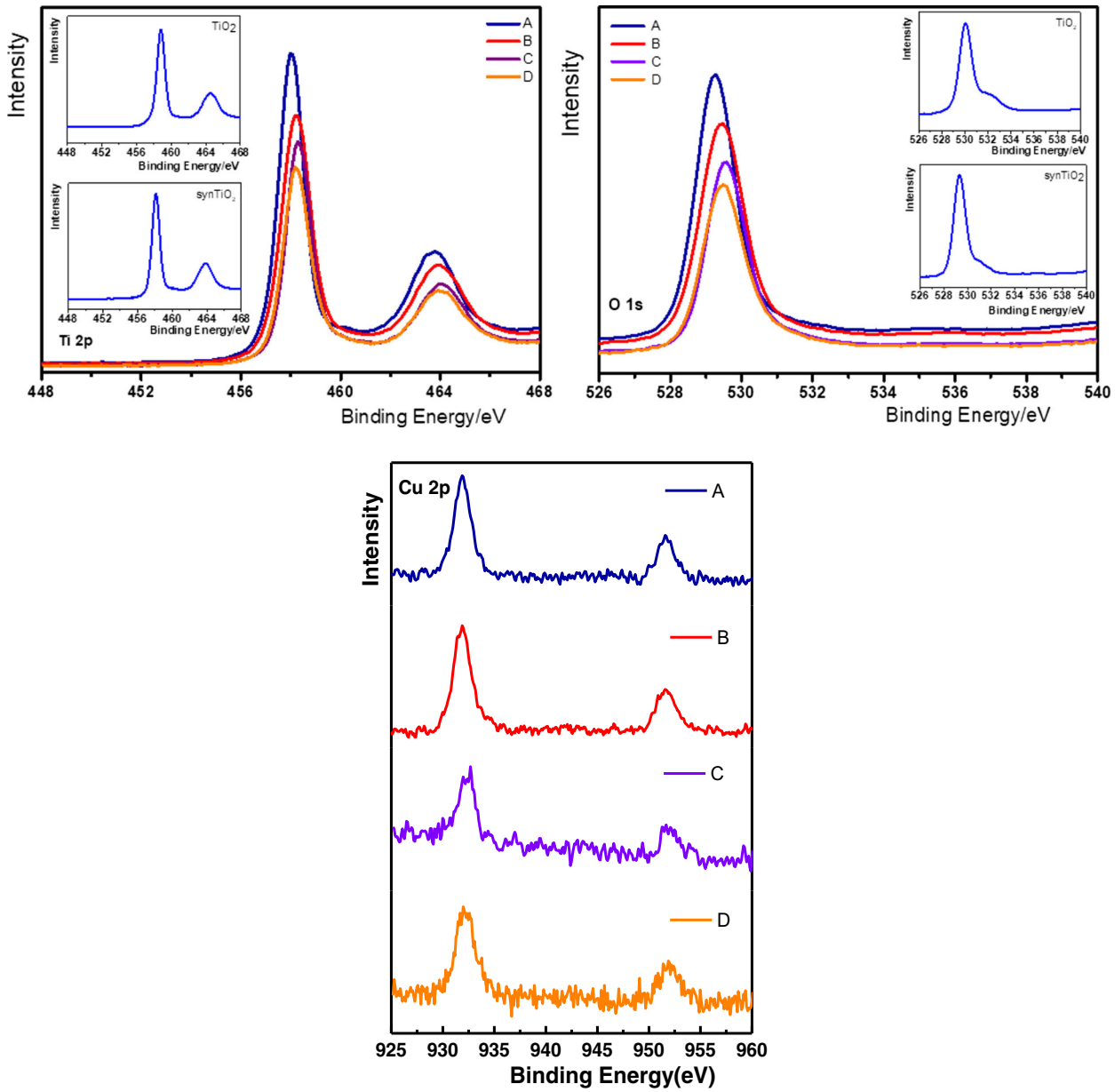

Fig. 2 XPS spectra (A) 0.25%Cu-TiO_2, (B) 0.50%Cu-TiO_2, (C) 0.25%Cu-synTiO_2, and (D) 0.50%Cu-synTiO_2

constituted the key role of the high activity of TiO_2 P-25 powder.

N_2 adsorption-desorption isotherms of the specimens indicated type IV with a hysteresis loop associated with mesoporous materials according to IUPAC classification (SI, Part 2, Fig. 6) (Sing 1985). BET surface area measurements revealed that TiO_2 specimen would expose the highest surface area for interaction with 30 kDa humic components (Table 1). Cu doping decreased TiO_2 surface area. Although surface area of syn-TiO_2 was smaller than TiO_2, a non-consistent trend was attained with respect to increasing dopant concentration. Photocatalyst dose (0.25 mg/mL) dependent average exposed surface area was calculated as 0.626 $m^2 \pm 0.0666$.

Humic characterization

Thirty kilodaltons HA exhibited UV-vis parameters (cm^{-1}) as $Color_{436} = 0.0603$, $UV_{365} = 0.1413$, $UV_{280} = 0.3373$, $UV_{254} = 0.3973$, and DOC as 4.38 mg/L. FI was 1.12 displaying the dominance of humic fluorophores (FI ≤ 1.4) in comparison to microbially derived organic fractions (FI ≥ 1.9) (Sen Kavurmaci and Bekbolet 2014). Based on EEM contour plots, fluorescence features of HA distinctly

Table 2 Kinetics of photocatalytic degradation of humic acid

Photocatalyst specimen	Pseudo first order kinetic reaction constant, k, $\times 10^{-2}$, min^{-1}				
	UV-vis spectroscopic parameters				DOC
	$Color_{436}$	UV_{365}	UV_{280}	UV_{254}	
TiO_2	0.795	0.762	0.730	0.692	0.575
$synTiO_2$	1.136	1.246	1.237	1.214	0.515
0.25% Cu-TiO_2	0.624	0.855	1.03	1.06	1.32
0.50% Cu-TiO_2	1.24	1.52	1.57	1.58	0.570
0.25% Cu-$synTiO_2$	0.650	0.732	0.770	0.775	0.852
0.50% Cu-$synTiO_2$	0.795	0.762	0.730	0.692	0.575

expressed the presence of humic-like and fulvic-like fluorophores excluding other regional speciation (Birben et al. 2015).

Photocatalytic degradation kinetics

Based on the irradiation time-dependent logarithmic decay profiles, photocatalytic degradation of HA was approximated to pseudo first-order kinetic model ($R^2 > 0.80$) (Table 2).

Photocatalytic mineralization extents (DOC, k, min^{-1}) revealed a faster removal upon use of 0.25% Cu-TiO_2 in comparison to 0.25% Cu-$synTiO_2$ > 0.50% Cu-$synTiO_2$ = TiO_2 > 0.50% Cu-TiO_2 > $synTiO_2$. Further evaluation with respect to half-life condition was presented in SI, Part 4, Fig. 8.

Upon pH dependent zeta potential measurements, pH_{zpc} of TiO_2 was determined as 5.67 (Mandzy et al. 2005). Presence of Cu dopant shifted pH_{zpc} to 6.54 for 0.25% Cu-TiO_2 and 6.47 for 0.50% Cu-TiO_2. pH_{zpc} of syn-TiO_2 was 4.91 and upon doping with Cu, a slight decrease was observed as pH_{zpc}:4.52 for 0.25% Cu-$synTiO_2$ and 4.42 for 0.50% Cu-$synTiO_2$. Similar result was attained for synthesized TiO_2 nanoparticles as pH_{zpc} = 5.1; however, a shift to higher pH conditions was reported via 1–3% Cu doping (Sahu et al. 2011).

Upon introduction to aqueous medium, TiO_2 would be dispersed and hydrated surface would acquire charge through deprotonation and protonation of the surface groups.

$$TiO_2 + H_2O \rightarrow Ti^{IV}{-}OH + H^+$$
$$Ti^{IV}{-}OH + H^+ \rightarrow TiOH_2{}^+ \quad pH < pH_{zpc}$$
$$Ti^{IV}{-}OH \rightarrow Ti{-}O^- + H^+ \quad pH > pH_{zpc}$$

In a similar manner, Cu-doped TiO_2 would also exhibit positively and negatively charged surface sites depending on the respective pH_{zpc} conditions

$$Ti{-}O{-}Cu_2 + H_2O \rightarrow TiOH{-}O(H){-}Cu_2$$
$$Ti{-}O(H){-}Cu_2 \rightarrow TiO^-{-}Cu_2 + H^+ \quad pH > pH_{zpc}$$
$$Ti{-}O(H){-}Cu_2 \rightarrow Ti{-}OH_2{}^+{-}Cu_2 + H^+ \quad pH < pH_{zpc}$$

Due to surface oriented nature of photocatalysis, electrostatic interactions between the pH_{zpc} dependent oppositely charged photocatalyst surface sites and negatively charged humic components should be encountered. Since all reactions were performed under neutral pH conditions (pH~7), deprotonated humic carboxylic functional groups (pH = 3–5) should be attracted to the positively charged oxide surface sites. Regarding pH_{zpc} conditions of the photocatalyst specimens and prevailing neutral pH conditions, all of the TiO_2 specimens would acquire positively and negatively charged sites open to

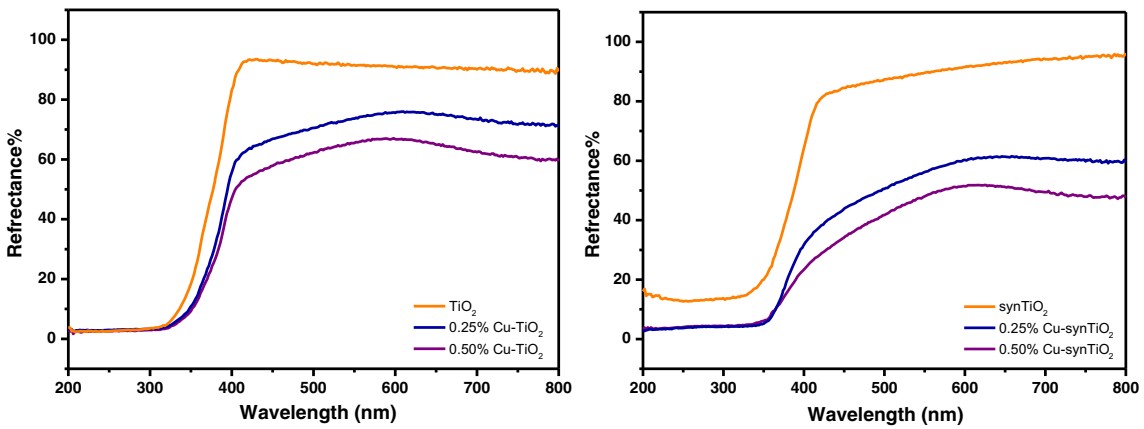

Fig. 3 UV-DRS spectra of TiO_2 specimens

electrostatic interactions with the negatively charged humic sub-fractions due to deprotonation of the carboxylic groups. It should also be indicated that besides electrostatic interactions, hydrogen bonding, chelation and charge-transfer complexation could also play specific roles during initial adsorption process as well as during photocatalysis.

Zeta potential measurements of the reaction consortium composed of humic sub-fractions and photocatalyst specimens expressed quite similar values as an average of -28.81 ± 0.46 mV indicating negative overall surface charge. This charge reversal on the TiO_2 surface could also lead to repulsion of negatively charged humic moieties; however, an enhanced attraction could be expected towards positively charged centers of TiO_2 particles. No direct explanation could be expressed between the removal efficiencies of the humic UV-vis parameters and DOC upon use of all specimens except TiO_2. The reason could be attributed to the initial adsorption of 30 kDa humic components onto photocatalyst specimens prior to the initiation of the light

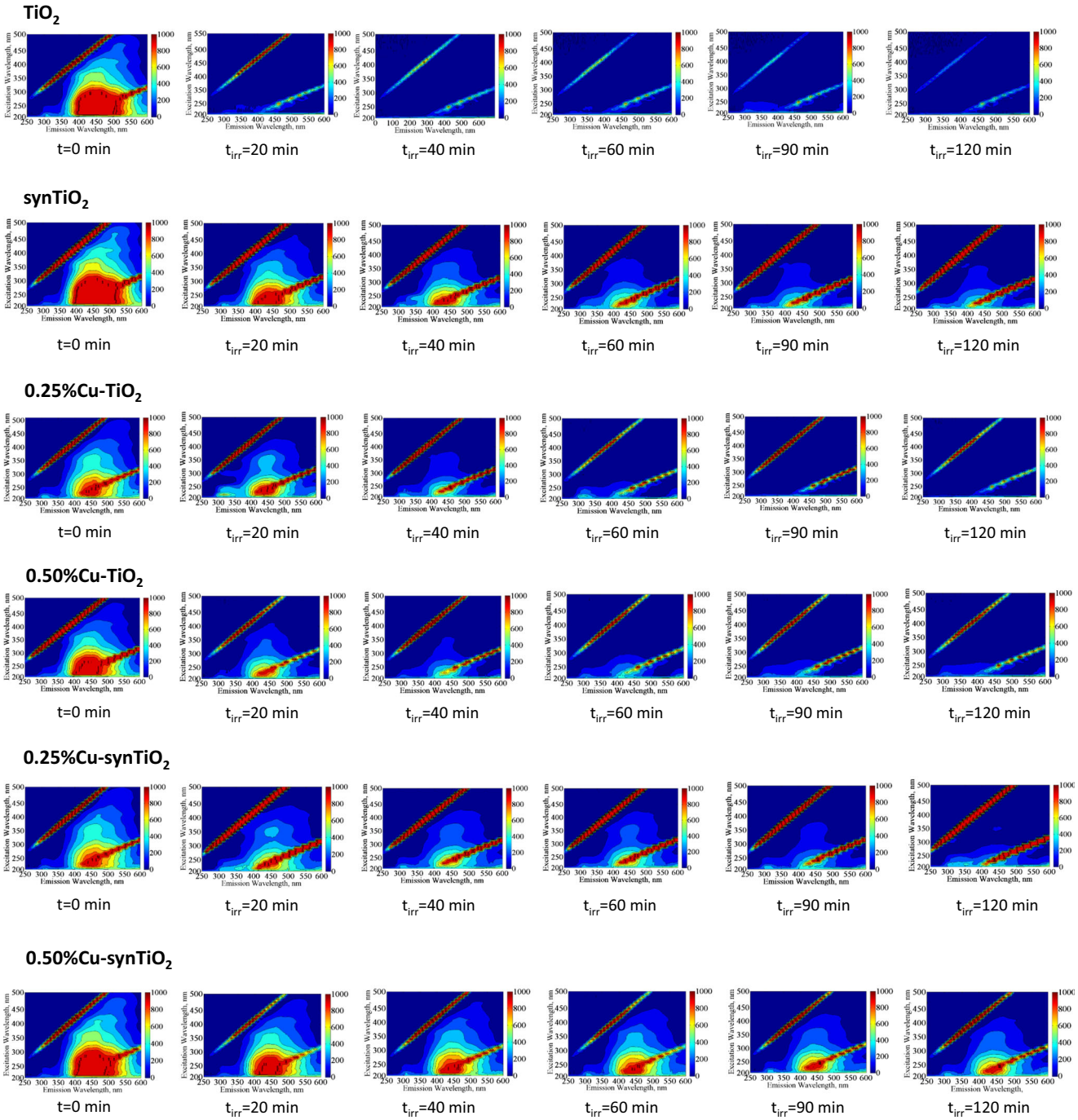

Fig. 4 Irradiation time-dependent EEM fluorescence contour plots

exposure (SI, Part 4, Fig. 9). The role of Cu doping of TiO_2 could only be related to unresolved reaction pathways.

UV-vis and fluorescence spectroscopic evaluation of humic acids

Besides, kinetics of HA descriptive parameters, carbon-based UV-vis parameters also hold prime importance revealing information with respect to organic carbon contents. $CbUV_{254}$ also defined as $SUVA_{254}$ displays extent of aromaticity change during treatment (Frimmel and Abbt-Braun 2009; Uyguner and Bekbolet 2005). Following an irradiation period of 60 min, sequence of $CbUV_{254}$ was 0.50% Cu-synTiO_2 > 0.25% Cu-synTiO_2 > 0.25% Cu-TiO_2 > 0.25% Cu-synTiO_2 > synTiO_2 > 0.50% CuTiO_2 > TiO_2. Color forming moieties were more preferentially removed with respect to DOC (SI, Part 4, Fig. 10).

SFI values could not be directly related to FI values displaying the presence and role of non-fluorescent humic components. Irradiation time dependent sample specific EEM contour plots could be simply expressed as follows (Fig. 4):

TiO_2: no significant regional fluorophores, i.e., humic-like and fulvic-like were recorded even for the early stages of irradiation, however, presence of Region I and Region II were seen even after t_{irr} = 90 min.

synTiO_2: for t_{irr} = 60 min along with the removal of humic-like and fulvic-like fluorophores a shift to Regions I and II was recorded.

0.25% Cu-TiO_2: for t_{irr} = 60 min along with the removal of humic-like and fulvic-like fluorophores a shift to Regions I and II was recorded. Further irradiation periods resulted in complete removal fluorophores.

0.50% Cu-TiO_2: for prolonged irradiation periods, existence of Regions I and II were evident expressing formation of lower molecular weight fractions.

0.25% Cu-synTiO_2: for t_{irr} = 120 min humic-like and fulvic-like fluorophores were still evident along including a shift to Regions I and II.

0.50% Cu-synTiO_2: for prolonged irradiation periods, e.g., 120 min all regions excluding Region III were still present.

EEM fluorescence features of humics could not be directly related to the removal of UV_{254} and DOC. Through adsorptive fractionation, the remaining organics onto the photocatalyst specimens could proceed a different degradation mechanism with respect to the humic fractions remaining in solution. Initial adsorption of the humics onto oxide surfaces lead to fractionation of humic components preferentially aromatic domains (Lee et al. 2015). During photocatalysis, a continuous adsorption-desorption process takes place between diverse groups of humic components comprised of untreated, partially oxidized, defragmented, re-assembled fractions etc. and the exposed surface area of the photocatalyst specimens. Reactivities of these groups could also pose different fluorophoric properties expressing diverse reaction mechanisms (Phong and Hur 2015). Based on the attained kinetic data, the remaining UV_{254} and DOC composition of the treated samples could not be directly related to the presence and absence of the fluorophoric Regions I–V. Fluorescent humic is mainly composed of relatively small units (< 2000 Da) held together by weak forces (Romera-Castillo et al. 2014). This could also be related to the formation of lower molecular size fraction via photocatalysis through oxidative degradation (Bekbolet and Sen-Kavurmaci 2015). Fluorescence quenching could also take place between protein-like and humic-like fluorophores forming new centers of attraction for both adsorptive and oxidative interactions (Wang et al. 2015). It should also be indicated that, for every fluorophore present in humic composition, there might be non-fluorophoric components contributing to the spectroscopic properties and DOC of the treated solution matrix.

Conclusion

In this study, TiO_2 P-25 was taken as a commercial sample, sol-gel prepared TiO_2 and respective Cu-doped specimens were prepared by incipient wet impregnation method. All specimens were employed for degradation of 30 kDa molecular size fraction of humic acid.

All photocatalyst specimens were characterized by XRD, SEM, XPS, Raman, UV-vis DRS, and BET techniques. pH_{zpc} were determined by pH-dependent zeta potential measurements and E_{bg} conditions were presented. Morphological properties expressed anatase phase dominance in Cu-doped synTiO_2 specimens in comparison to mixed phase of TiO_2. Cu doping was interpreted as substitutional.

Humic properties were expressed by UV-vis and advanced fluorescence spectroscopic parameters as well as DOC.

Upon photocatalytic treatment under solar light irradiation, based on the obtained UV-vis parameters and DOC removal data, 0.25% Cu-doped samples showed slightly higher photocatalytic performance with regard to undoped specimens as P-25 and sol-gel synthesized TiO_2. With respect to the mineralization extents (first order kinetic constant, min^{-1}), photocatalytic performance of the TiO_2 specimens were found to be as follows: 0.25% Cu-TiO_2 > 0.25% Cu-synTiO_2 > 0.50% Cu-synTiO_2 = TiO_2 > 0.50% Cu-TiO_2 > synTiO_2.

Consequently, sample-specific removal efficiencies of UV-vis parameters were obtained.

Following photocatalysis, remaining organic matrix as elucidated by EEM fluorescence features expressed the removal of higher molecular size fractions expressing humic-like and fulvic-like fluorophores.

Based on the attained results, it is highly recommended that in case of complex organic substrate, the role of dopants should be more clearly elucidated by sophisticated methodologies from better understanding point of view.

Acknowledgements The authors are thankful to Prof Neren Okte, Bogazici University, Chemistry Department, for BET and UV-DRS measurements. The authors are also thankful to Assoc. Prof. Serap Acar Derman, Yildiz Technical University, Department of Bioengineering for zeta potential measurements.

Funding information Financial support provided by the Research Fund of Bogazici University through Project No: 13381 is gratefully acknowledged.

References

Aguilar T, Navas J, Alcántara R, Fernández-Lorenzo C, Gallardo JJ, Blanco G, Martín-Calleja J (2013) A route for the synthesis of cu-doped TiO_2 nanoparticles with a very low band gap. Chem Phys Lett 571:49–53. https://doi.org/10.1016/j.cplett.2013.04.007

Ahmad J, Siddiqui MA, Akhtar MJ, Alhadlaq HA, Alshamsan A, Khan ST, Wahab R, Al-Khedhairy AA, Al-Salim A, Musarrat J, Saquib Q, Fareed M, Ahamed M (2018) Copper doping enhanced the oxidative stress–mediated cytotoxicity of TiO_2 nanoparticles in A549 cells. Human Exp Toxicol 37:496–507. https://doi.org/10.1177/0960327117714040

Araña J, Fernández Rodríguez C, González Díaz O, Herrera Melián JA, Pérez Peña J (2005) Role of Cu in the Cu-TiO_2 photocatalytic degradation of dihydroxybenzenes. Catal Today 101:261–266. https://doi.org/10.1016/j.cattod.2005.03.006

Banerjee S, Pillai SC, Falaras P, O'Shea KE, Byrne JA, Dionysiou DD (2014) New insights into the mechanism of visible light photocatalysis. J Phys Chem Lett 5:2543–2554. https://doi.org/10.1021/jz501030x

Bashiri R, Mohamed NM, Kait CF, Sufian S (2015) Hydrogen production from water photosplitting using Cu/TiO_2 nanoparticles: effect of hydrolysis rate and reaction medium. Int J Hydrog Energy 40:6021–6037. https://doi.org/10.1016/j.ijhydene.2015.03.019

Bekbolet M, Sen-Kavurmaci S (2015) The effect of photocatalytic oxidation on molecular size distribution profiles of humic acid. Photochem Photobiol Sci 14:576–582. https://doi.org/10.1039/C4PP00262H

Bensouici F, Bououdin M, Dakhel AA, Tala-Ighil R, Tounane M, Iratni A, Souier T, Liu S, Cai W (2017) Optical, structural and photocatalysis properties of cu-doped TiO_2 thin films. Appl Surf Sci 395:110–116. https://doi.org/10.1016/j.apsusc.2016.07.034

Birben NC, Uyguner-Demirel CS, Sen-Kavurmaci S, Gurkan YY, Turkten N, Cinar Z, Bekbolet M (2015) Comparative evaluation of anion doped photocatalysts on the mineralization and decolorization of natural organic matter. Catalysis Today 240(Part A):125–131. https://doi.org/10.1016/j.cattod.2014.04.020

Biyoghe Bi Ndong L, Ibondou MP, Gu X, Lu S, Qiu Z, Sui Q, Mbadinga SM (2014) Enhanced photocatalytic activity of TiO_2 nanosheets by doping with Cu for chlorinated solvent pollutants degradation. Ind Eng Chem Res 53:1368–1376. https://doi.org/10.1021/ie403405z

Boccuzzi F, Chiorino A, Gargano M, Ravasio N (1997) Preparation, characterization, and activity of Cu/TiO_2 catalysts. II. Effect of the catalyst morphology on the hydrogenation of 1,3-cyclooctadiene and the CO–NO reaction on Cu/TiO_2 catalysts. J Catal 165:140–149. https://doi.org/10.1006/jcat.1997.1476

Bokhimi X, Morales A, Novaro O, López T, Chimal O, Asomoza M, Gómez R (1997) Effect of copper precursor on the stabilization of titania phases, and the optical properties of Cu/TiO_2 prepared with the sol–gel technique. Chem Mater 9:2616–2620. https://doi.org/10.1021/cm970279r

Byrne C, Fagan R, Hinder S, McCormack DE, Pillai SC (2016) New approach of modifying the anatase to rutile transition temperature in TiO_2 photocatalysts. RSC Adv 6:95232–95238. https://doi.org/10.1039/C6RA19759K

Cao X, Tao J, Xiao X, Nan J (2018) Hydrothermal-assisted synthesis of the multi-element-doped TiO_2 micro/nanostructures and their photocatalytic reactivity for the degradation of tetracycline hydrochloride under the visible light irradiation. J Photochem Photobiol A Chem 364:202–207. https://doi.org/10.1016/j.jphotochem.2018.06.013

Carvalho HWP, Rocha MVJ, Hammer P, Ramalho TC (2013) TiO_2–Cu photocatalysts: a study on the long- and short-range chemical environment of the dopant. J Mater Sci 48:3904–3912. https://doi.org/10.1007/s10853-013-7192-1

Chelli VR, Golder AK (2017) Bimetal doping on TiO_2 for photocatalytic water treatment: a green route. Eur Water 58

Ci Y, Wang S, Zhang X, Fang Z, Ma A, Huang Z (2018) Chemical warfare agents' degradation on Fe–Cu codoped kaTiO_2 nanoparticles. Appl Phys A 124:786. https://doi.org/10.1007/s00339-018-2209-x

Coloma F, Marquez F, Rochester CH, Anderson JA (2000) Determination of the nature and reactivity of copper sites in Cu–TiO_2 catalysts. Phys Chem Chem Phys 2:5320–5327. https://doi.org/10.1039/B005331G

Colón G, Maicu M, Hidalgo MC, Navío JA (2006) Cu-doped TiO_2 systems with improved photocatalytic activity. Appl Catal B Environ 67:41–51. https://doi.org/10.1016/j.apcatb.2006.03.019

Dong J, Ye J, Ariyanti D, Wang Y, Wei S, Gao W (2018) Enhancing photocatalytic activities of titanium dioxide via well-dispersed copper nanoparticles. Chemosphere 204:193–201. https://doi.org/10.1016/j.chemosphere.2018.04.012

Dorraj M, Alizadeh M, Sairi NA, Basirun WJ, Goh BT, Woi PM, Alias Y (2017) Enhanced visible light photocatalytic activity of copper-doped titanium oxide–zinc oxide heterojunction for methyl orange degradation. Appl Surf Sci 414:251–261. https://doi.org/10.1016/j.apsusc.2017.04.045

Dorraj M, Goh BT, Sairi NA, Woi PM, Basirun WJ (2018) Improved visible-light photocatalytic activity of TiO_2 co-doped with copper and iodine. Appl Surf Sci 439:999–1009. https://doi.org/10.1016/j.apsusc.2017.12.248

Etacheri V, Di Valentin C, Schneider J, Bahnemann D, Pillai SC (2015) Visible-light activation of TiO_2 photocatalysts: advances in theory and experiments. J Photochem Photobiol C: Photochem Rev 25:1–29. https://doi.org/10.1016/j.jphotochemrev.2015.08.003

Fagan R, McCormack DE, Dionysiou DD, Pillai SC (2016) A review of solar and visible light active TiO_2 photocatalysis for treating bacteria, cyanotoxins and contaminants of emerging concern. Mater Sci Semicond Process 42:2–14. https://doi.org/10.1016/j.mssp.2015.07.052

Fisher MB, Keane DA, Fernández-Ibáñez P, Colreavy J, Hinder SJ, McGuigan KG, Pillai SC (2013) Nitrogen and copper doped solar light active TiO_2 photocatalysts for water decontamination. Appl Catal B Environ 130-131:8–13. https://doi.org/10.1016/j.apcatb.2012.10.013

Frimmel FH, Abbt-Braun G (2009) Dissolved organic matter (DOM) in natural environments. In: Senesi N, Xing B, Huang PM (eds) Biophysico-chemical processes involving natural nonliving organic matter in environmental systems. https://doi.org/10.1002/9780470494950.ch10

Guo MY, Liu F, Leung YH, He Y, Ng AMC, Djurišić AB, Li H, Shih K, Chan WK (2017) Annealing-induced antibacterial activity in TiO_2 under ambient light. J Phys Chem C 121:24060–24068. https://doi.org/10.1021/acs.jpcc.7b07325

Hirota K-I, Maeda M (2017) Copper and nitrogen co-doping effect on visible-light responsive photocatalysis of plasma-nitrided copper-doped titanium oxide film. J Mater Sci Chem Eng 5:52–62. https://doi.org/10.4236/msce.2017.512005

Hu Q, Huang J, Li G, Chen J, Zhang Z, Deng Z, Jiang Y, Guo W, Cao Y (2016) Effective water splitting using CuO_x/TiO_2 composite films: role of Cu species and content in hydrogen generation. Appl Surf Sci 369:201–206. https://doi.org/10.1016/j.apsusc.2016.01.281

Ilkhechi NN, Kaleji BK (2014) High temperature stability and photocatalytic activity of nanocrystalline anatase powders with Zr and Si co-dopants. J Sol-Gel Sci Technol 69:351–356. https://doi.org/10.1007/s10971-013-3224-1

Ilkhechi NN, Kaleji BK, Salahi E, Hosseinabadi N (2015) Comparison of optical and structural properties of Cu doped and Cu/Zr co-doped TiO_2 nanopowders calcined at various temperatures. J Sol-Gel Sci Technol 74:765–773. https://doi.org/10.1007/s10971-015-3661-0

Jaiswal R, Bharambe J, Patel N, Dashora A, Kothari DC, Miotello A (2015) Copper and nitrogen co-doped TiO_2 photocatalyst with enhanced optical absorption and catalytic activity. Appl Catal B Environ 168-169:333–341. https://doi.org/10.1016/j.apcatb.2014.12.053

Jo W-K, Jin Y-J (2018) 2D graphene-assisted low-cost metal (Ag, Cu, Fe, or Ni)-doped TiO_2 nanowire architectures for enhanced hydrogen generation. J Alloys Compd 765:106–112. https://doi.org/10.1016/j.jallcom.2018.06.181

Jung M, Hart JN, Scott J, Ng YH, Jiang Y, Amal R (2016) Exploring Cu oxidation state on TiO_2 and its transformation during photocatalytic hydrogen evolution. Appl Catal A Gen 521:190–201. https://doi.org/10.1016/j.apcata.2015.11.013

Karunakaran C, Abiramasundari G, Gomathisankar P, Manikandan G, Anandi V (2010) Cu-doped TiO_2 nanoparticles for photocatalytic disinfection of bacteria under visible light. J Colloid Interface Sci 352:68–74. https://doi.org/10.1016/j.jcis.2010.08.012

Kerc A, Bekbolet M, Saatci AM (2004) Effects of oxidative treatment techniques on molecular size distribution of humic acids. Water Sci Technol 49:7–12. https://doi.org/10.2166/wst.2004.0205

Khraisheh M, Wu L, Al-Muhtaseb AH, Al-Ghouti MA (2015) Photocatalytic disinfection of *Escherichia coli* using TiO_2 P25 and Cu-doped TiO_2. J Ind Eng Chem 28:369–376. https://doi.org/10.1016/j.jiec.2015.02.023

Kumar SG, Devi LG (2011) Review on modified TiO_2 photocatalysis under UV/visible light: selected results and related mechanisms on interfacial charge carrier transfer dynamics. J Phys Chem A 115:13211–13241. https://doi.org/10.1021/jp204364a

Kumar PD, Lakshmana Reddy N, Srinivas B, Durgakumari V, Roddatis V, Bondarchuk Karthik M, Ikuma Y, Shankar MV (2016) Stable and active Cu_xO/TiO_2 nanostructured catalyst for proficient hydrogen production under solar light irradiation. Sol Energy Mater Sol Cells 146:63–71. https://doi.org/10.1016/j.solmat.2015.11.030

Lee B-M, Seo Y-S, Hur J (2015) Investigation of adsorptive fractionation of humic acid on graphene oxide using fluorescence EEM-PARAFAC. Water Res 73:242–251. https://doi.org/10.1016/j.watres.2015.01.020

Leyland NS, Podporska-Carroll J, Browne J, Hinder SJ, Quilty B, Pillai SC (2016) Highly efficient F, Cu doped TiO_2 anti-bacterial visible light active photocatalytic coatings to combat hospital-acquired infections. Sci Rep 6:24770. https://doi.org/10.1038/srep24770

Li Bassi AL, Cattaneo D, Russo V, Bottani CE, Barborini E, Mazza T, Piseri P, Milani P, Ernst FO, Wegner K, Pratsinis SE (2005) Raman spectroscopy characterization of titania nanoparticles produced by flame pyrolysis: the influence of size and stoichiometry. J Appl Phys 98:074305. https://doi.org/10.1063/1.2061894

Lin JC-T, Sopajaree K, Jitjanesuwan T, Lu M-C (2018) Application of visible light on copper-doped titanium dioxide catalyzing degradation of chlorophenols. Sep Purif Technol 191:233–243. https://doi.org/10.1016/j.seppur.2017.09.027

López R, Gómez R, Llanos ME (2009) Photophysical and photocatalytic properties of nanosized copper-doped titania sol–gel catalysts. Catal Today 148:103–108. https://doi.org/10.1016/j.cattod.2009.04.001

Mahmoud MS, Ahmed E, Farghali AA, Zaki AH, Abdelghani EAM, Barakat NAM (2018) Influence of Mn, Cu, and Cd–doping for titanium oxide nanotubes on the photocatalytic activity toward water splitting under visible light irradiation. Colloids Surf A Physicochem Eng Asp 554:100–109. https://doi.org/10.1016/j.colsurfa.2018.06.039

Mandzy N, Grulke E, Druffel T (2005) Breakage of TiO_2 agglomerates in electrostatically stabilized aqueous dispersions. Powder Technol 160:121–126. https://doi.org/10.1016/j.powtec.2005.08.020

Mathew S, Ganguly P, Rhatigan S, Kumaravel V, Byrne C, Hinder S, Bartlett J, Nolan M, Pillai SC (2018) Cu-doped TiO_2: visible light assisted photocatalytic antimicrobial activity. Appl Sci 8:2067. https://doi.org/10.3390/app8112067

Moongraksathum B, Shang J-Y, Chen Y-W (2018) Photocatalytic antibacterial effectiveness of cu-doped TiO_2 thin film prepared via the peroxo sol-gel method. Catalysts 8:352. https://doi.org/10.3390/catal8090352

Ohno T, Sarukawa K, Tokieda K, Matsumura M (2001) Morphology of a TiO_2 photocatalyst (Degussa, P-25) consisting of anatase and rutile crystalline phases. J Catal 203:82–86. https://doi.org/10.1006/jcat.2001.3316

Pava-Gómez B, Vargas-Ramírez X, Díaz-Uribe C (2018) Physicochemical study of adsorption and photodegradation processes of methylene blue on copper-doped TiO_2 films. J Photochem Photobiol A Chem 360:13–25. https://doi.org/10.1016/j.jphotochem.2018.04.022

Pelaez M, Nolan NT, Pillai SC, Seery MK, Falaras P, Kontos AG, Dunlop PSM, Hamilton JWJ, Byrne JA, O'Shea K, Entezari MH, Dionysiou DD (2012) A review on the visible light active titanium dioxide photocatalysts for environmental applications. Appl Catal B Environ 125:331–349. https://doi.org/10.1016/j.apcatb.2012.05.036

Phong DD, Hur J (2015) Insight into photocatalytic degradation of dissolved organic matter in UVA/TiO_2 systems revealed by fluorescence EEM-PARAFAC. Water Res 87:119–126. https://doi.org/10.1016/j.watres.2015.09.019

Polliotto V, Livraghi S, Krukowska A, Dozzi MV, Zaleska-Medynska A, Selli E, Giamello E (2018) Copper-modified TiO_2 and $ZrTiO_4$: Cu oxidation state evolution during photocatalytic hydrogen production. ACS Appl Mater Interfaces 10:27745–27756. https://doi.org/10.1021/acsami.8b05528

Pongwan P, Wetchakun K, Phanichphant S, Wetchakun N (2016) Enhancement of visible-light photocatalytic activity of Cu-doped TiO_2 nanoparticles. Res Chem Intermed 42:2815–2830. https://doi.org/10.1007/s11164-015-2179-y

Reda SM, Khairy M, Mousa MA (2017) Photocatalytic activity of nitrogen and copper doped TiO_2 nanoparticles prepared by microwave-assisted sol-gel process. Arabian J Chem. https://doi.org/10.1016/j.arabjc.2017.02.002 open access

Romera-Castillo C, Chen M, Yamashita Y, Jaffé R (2014) Fluorescence characteristics of size-fractionated dissolved organic matter: implications for a molecular assembly based structure? Water Res 55:40–51. https://doi.org/10.1016/j.watres.2014.02.017

Sahu M, Suttiponparnit K, Suvachittanont S, Charinpanitkul T, Biswas P (2011) Characterization of doped TiO_2 nanoparticle dispersions. Chem Eng Sci 66:3482–3490. https://doi.org/10.1016/j.ces.2011.04.003

Sen Kavurmaci S, Bekbolet M (2014) Tracing TiO_2 photocatalytic degradation of humic acid in the presence of clay particles by excitation–emission matrix (EEM) fluorescence spectra. J Photochem Photobiol A Chem 282:53–61. https://doi.org/10.1016/j.jphotochem.2014.03.011

Sing KSW (1985) Reporting physisorption data for gas/solid systems with special reference to the determination of surface area and

porosity. (Recommendations 1984) vol 57. https://doi.org/10.1351/pac198557040603

Tercero Espinoza LA, ter Haseborg E, Weber M, Karle E, Peschke R, Frimmel FH (2011) Effect of selected metal ions on the photocatalytic degradation of bog lake water natural organic matter. Water Res 45:1039–1048. https://doi.org/10.1016/j.watres.2010.10.013

Tseng IH, Chang W-C, Wu JCS (2002) Photoreduction of CO_2 using sol–gel derived titania and titania-supported copper catalysts. Appl Catal B Environ 37:37–48. https://doi.org/10.1016/S0926-3373(01)00322-8

Turkten N, Cinar Z (2017) Photocatalytic decolorization of azo dyes on TiO_2: prediction of mechanism via conceptual DFT. Catal Today 287:169–175. https://doi.org/10.1016/j.cattod.2017.01.019

Unwiset P, Makdee A, Chanapattharapol KC, Kidkhunthod P (2018) Effect of Cu addition on TiO_2 surface properties and photocatalytic performance: X-ray absorption spectroscopy analysis. J Phys Chem Solids 120:231–240. https://doi.org/10.1016/j.jpcs.2018.05.003

Uyguner CS, Bekbolet M (2004) Photocatalytic degradation of natural organic matter: kinetic considerations and light intensity dependence. International Journal of Photoenergy 6:73–80. https://doi.org/10.1155/s1110662x0400011x

Uyguner CS, Bekbolet M (2005) Evaluation of humic acid photocatalytic degradation by UV–vis and fluorescence spectroscopy. Catal Today 101:267–274. https://doi.org/10.1016/j.cattod.2005.03.011

Uyguner CS, Bekbolet M (2007) Contribution of metal species to the heterogeneous photocatalytic degradation of natural organic matter. Int J Photoenergy 2007:Article ID 23156. https://doi.org/10.1155/2007/23156

Uyguner CS, Bekbolet M (2010) TiO_2-assisted photocatalytic degradation of humic acids: effect of copper ions. Water Sci Technol 61:2581–2590. https://doi.org/10.2166/wst.2010.174

Uyguner-Demirel CS, Bekbolet M (2011) Significance of analytical parameters for the understanding of natural organic matter in relation to photocatalytic oxidation. Chemosphere 84:1009–1031. https://doi.org/10.1016/j.chemosphere.2011.05.003

Wang Z, Cao J, Meng F (2015) Interactions between protein-like and humic-like components in dissolved organic matter revealed by fluorescence quenching. Water Res 68:404–413. https://doi.org/10.1016/j.watres.2014.10.024

Wang M, Peng L, Wang J, Li C, Guan L, Lin Y (2018) Enhanced visible light photocatalytic decolorization of methylene blue by hierarchical ternary nanocomposites Cu-TiO_2-mesoporous-silica microsphere. J Nanosci Nanotechnol 18:8269–8275. https://doi.org/10.1166/jnn.2018.16405

Xu Y-H, Liang D-H, M-l L, Liu D-Z (2008) Preparation and characterization of Cu_2O–TiO_2: efficient photocatalytic degradation of methylene blue. Mater Res Bull 43:3474–3482. https://doi.org/10.1016/j.materresbull.2008.01.026

Yadav HM, Otari SV, Koli VB, Mali SS, Hong CK, Pawar SH, Delekar SD (2014) Preparation and characterization of copper-doped anatase TiO_2 nanoparticles with visible light photocatalytic antibacterial activity. J Photochem Photobiol A Chem 280:32–38. https://doi.org/10.1016/j.jphotochem.2014.02.006

Yang X-J, Wang S, Sun H-M, Wang X-B, Lian J-S (2015) Preparation and photocatalytic performance of Cu-doped TiO_2 nanoparticles. Trans Nonferrous Metals Soc China 25:504–509. https://doi.org/10.1016/S1003-6326(15)63631-7

Zhang M, Sun R, Li Y, Shi Q, Xie L, Chen J, Xu X, Shi H, Zhao W (2016) High H_2 evolution from quantum Cu(II) nanodot-doped two-dimensional ultrathin TiO_2 nanosheets with dominant exposed {001} facets for reforming glycerol with multiple electron transport pathways. J Phys Chem C 120:10746–10756. https://doi.org/10.1021/acs.jpcc.6b01030

Zheng X, Shen Z-P, Cheng C, Shi L, Cheng R, Yuan D-H (2018) Photocatalytic disinfection performance in virus and virus/bacteria system by Cu-TiO_2 nanofibers under visible light. Environ Pollut 237:452–459. https://doi.org/10.1016/j.envpol.2018.02.074

Zhou M, Yu J, Cheng B (2006) Effects of Fe-doping on the photocatalytic activity of mesoporous TiO_2 powders prepared by an ultrasonic method. J Hazard Mater 137:1838–1847. https://doi.org/10.1016/j.jhazmat.2006.05.028